https://doi.org/10.5194/nhess-2021-58
Preprint. Discussion started: 18 March 2021
© Author(s) 2021. CC BY 4.0 License.

Natural Hazards and Earth System Sciences
Discussions

The M_w 7.5 Tadine (Maré, Loyalty Is.) earthquake and related tsunami of December 5, 2018: implications for tsunami hazard assessment in New Caledonia.

Jean Roger[1,2*], Bernard Pelletier[3], Maxime Duphil[1], Jérôme Lefèvre[1], Jérôme Aucan[1], Pierre Lebellegard[3], Bruce Thomas[1,4], Céline Bachelier[5], David Varillon[5]

[1]ENTROPIE, Institut de Recherche pour le Développement, 101, Promenade Roger Laroque, BP A5 98848 Nouméa CEDEX, New Caledonia

[2]Now at: GNS Sciences, 1 Fairway Drive, Lower Hutt 5010, New Zealand

[3]GEOAZUR, Institut de Recherche pour le Développement, 101, Promenade Roger Laroque, BP A5 98848 Nouméa CEDEX, New Caledonia

[4]LISAH, Univ Montpellier, INRAE, IRD, Institut Agro, Montpellier, France

[5]IMAGO, Institut de Recherche pour le Développement, 101, Promenade Roger Laroque, BP A5 98848 Nouméa CEDEX, New Caledonia

Correspondence to: J. Roger (j.roger@gns.cri.nz)

Abstract. On the 5th of December 2018, a magnitude M_w 7.5 earthquake occurred southeast of Maré, an island of the Loyalty Archipelago, New Caledonia. This earthquake is located at the junction between the plunging Loyalty ridge and the southernmost Vanuatu arc, in a tectonically very active area regularly subjected to strong seismic crises and events higher than magnitude 7 and up to 8. Widely felt in New Caledonia it has been immediately followed by a tsunami warning, confirmed shortly after by a first wave arrival at the Loyalty Islands tide gauges (Maré and Lifou), then along the east coast of Grande Terre of New Caledonia and in several islands of the Vanuatu Archipelago. Seafloor initial deformation linked to tsunami generation has been modeled with MOST numerical code using earthquake parameters available from seismic observatories. Then the wave propagation has been modeled using SCHISM, another modelling code solving the shallow water equations on an unstructured grid based on a new regional DEM of ~180 m resolution and allowing refinement in many critical areas. Finally, the results have been compared to tide gauge records, field observations and testimonials from 2018. The arrival times, wave amplitude and polarities present good similarities, especially in far-field locations (Hienghène, Port-Vila and Poindimié). Maximum wave heights and energy maps for two different scenarios highlight the fact that the orientation of the source (strike of the rupture) played an important role, focusing the maximum energy path of the tsunami south of Grande-Terre and the Isle of Pines. However, both scenarios indicate similar propagation toward Aneityum, Vanuatu southernmost island, the bathymetry acting like a waveguide. This study has a significant implication in tsunami hazard mitigation in New Caledonia as it helps to validate the modelling code and process used to prepare a scenarios database for warning and coastal evacuation.

https://doi.org/10.5194/nhess-2021-58
Preprint. Discussion started: 18 March 2021
© Author(s) 2021. CC BY 4.0 License.

Natural Hazards and Earth System Sciences
Discussions
Open Access
EGU

1 General settings

1.1 Tectonic context

The December 5, 2018, M_w 7.5 earthquake is located southeast of Maré (Loyalty Islands, New Caledonia), immediately west of the southern New Hebrides/Vanuatu trench in the junction area between the Loyalty Ridge and the New Hebrides/Vanuatu arc (Figure 1). The Vanuatu trench and arc mark a segment of the convergence zone between the two major plates of the Southwest Pacific region (Australia and Pacific plates).

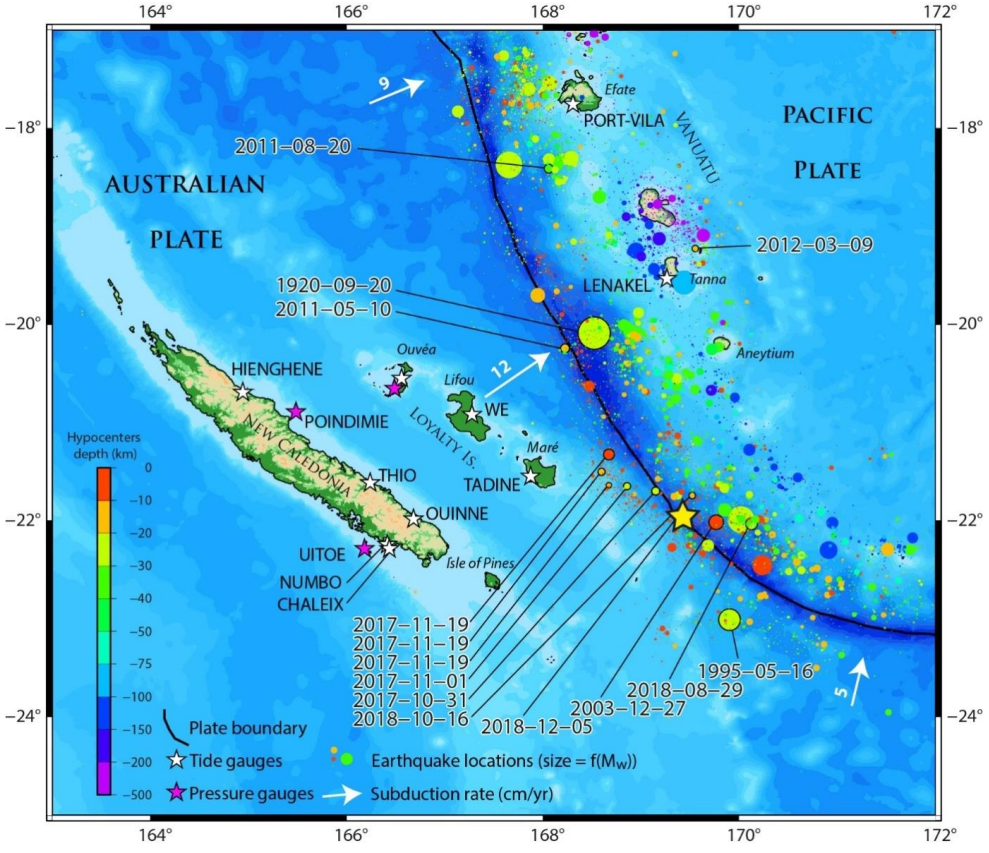

Figure 1: The New Caledonia/South Vanuatu Subduction zone. The colored dots represent the seismicity from the USGS database for the period January 1, 1900 to January 24, 2019, with size of dots proportional to event's magnitude. Tsunamigenic earthquakes having been recorded in New Caledonia (Roger et al., 2019b) are highlighted with dates. The white arrows symbolize the subduction directions and rates of the subducting Australian Plate under the Pacific plate. Tide and pressure gages able to record tsunami waves are respectively symbolized with white and purple stars. The yellow star locates the December 5, 2018 earthquake's epicenter.

The junction area around 22°S is very active tectonically (Monzier et al., 1984). The plunging Loyalty Ridge supported by the Australia Plate enters and partially clogs the trench. Considering the geometry of the Loyalty Ridge, the strike of the trench and the current orientation and rate of convergence (12 cm/y), the subduction/collision of the ridge tends to increase and would have started around 0.3 Ma (Monzier et al., 1990).

https://doi.org/10.5194/nhess-2021-58
Preprint. Discussion started: 18 March 2021
© Author(s) 2021. CC BY 4.0 License.

Natural Hazards and Earth System Sciences
Discussions

The data obtained by multibeam mapping and submersible diving (Daniel et al., 1986; Monzier et al., 1989 and 1990) at the junction zone (21.5°S and 22.2°S) indicate: 1) a spectacular collapse of the ridge as it approaches the trench (reef limestones affected by normal faulting are at 4,300 m deep), 2) a migration of the deformation front on the outer wall of the trench with the unusual presence of folds, 3) a narrowing and an eastward retreat of the trench by around 20 km relatively to its supposed initial position, 4) an uplift of the inner wall and 5) the development of E-W trending scarps suggesting left-lateral motion. The rapid variation of the convergence vector and the presence of numerous left-lateral strike-slip faulting earthquakes around 22°S, at the front of the junction zone and along or at the rear of the Matthew-Hunter arc segment, also suggest that the subduction/collision of the Loyalty Ridge causes the development of a new left-lateral plate boundary through the overlapping plate, connecting the trench to the spreading center of the North Fiji basin and thus isolating a microplate (the Matthew-Hunter microplate) at the southern end of the arc, strongly coupled to the Australian plate (Louat and Pelletier, 1989). The rate of motion on this transform fault zone was estimated by these authors at 10.5 cm/year. However, its precise geometry and location are not known, and several variants have been proposed (Louat and Pelletier, 1989; Maillet et al., 1989; Monzier, 1993; Patriat et al., 2015). As these authors have partially indicated, it is likely that this senestral shear zone is complex and that a bookshelf tectonic occurs at the southernmost part of the Vanuatu trench (21°S-23°S), by associating with the main senestral motion, dextral and extensive movements along NW-SE trending faults and pull-apart basins.

Series of GPS geodetic measurements on the Loyalty Ridge (Walpole, Mare, Lifou) and the Vanuatu arc (Matthew, Hunter, Aneityum, Tanna) sites from 1992 to 2000 have confirmed the presence of the left-lateral transform fault zone (Pelletier et al., 1998; Calmant et al., 2003). The data indicate that the convergence rate (Australia fixed) of 120 mm/year at N248° north of the ridge-arc junction (Tanna, Aneityum) is partitioned toward the south into a convergence rate of 50 mm/year perpendicular (N197°) to the trench (Matthew) and a senestral movement of 90 mm/year along an E-W trending transform zone, crosscutting the arc around 22°S and thus isolating the Matthew-Hunter microplate at the southern end of the arc (Calmant et al., 2003). In addition, GPS derived vectors of the New Caledonia sites are in good agreement with the movement of the Australian plate, suggesting therefore no significant intra-plate deformation between islands of the New Caledonian Archipelago. The termination of the southern Vanuatu back arc basins north of the junction zone, the increase in seismic activity and the shift towards the trench of the seismogenic zone in front of the junction zone, the short length of the Wadati-Benioff plane south of Aneityum (less than 200 km), the weak development of the volcanic arc at the front of the junction zone, the particular chemistry of the volcanism of the termination of the arc south of the ridge-arc junction (calco-alkaline magnesian and boninitic series) as well as the offset of the central spreading axis in the North Fiji basin have also been linked to the subduction/collision of the Loyalty Ridge (Monzier et al., 1984, 1990; Louat and Pelletier, 1989; Maillet et al., 1989; Monzier, 1993).

1.2 Seismicity at the Loyalty Ridge-Vanuatu Arc junction

The Loyalty island region and especially the Loyalty Ridge-Vanuatu Arc junction area around 22°S, 169.5°E is very active seismically. Nine large shallow earthquakes with magnitude equal or greater than seven occurred in this junction area since 1900. The largest was a M7.9 in August 9, 1901, located at 22°S, 170°E. A M7.6 earthquake occurred in March 16, 1928 at 170.24°E, 22.45°S. The seven others occurred during seismic crises in the last 40 years: a M_w7.4 in October 25, 1980; a M_w7.7 in May 16, 1995; a M_w7.3 in December 27, 2003; a

https://doi.org/10.5194/nhess-2021-58
Preprint. Discussion started: 18 March 2021
© Author(s) 2021. CC BY 4.0 License.

Natural Hazards and Earth System Sciences
Discussions

M_w7.1 in January 03, 2004; a M_w7.0 in November 29, 2017; a M_w7.1 in August 29, 2018 and a M_w7.5 in December 15, 2018. Among these seven M7+ events, four of them have occurred to the west of the trench, as the result of shallow normal faulting within the Australia downgoing plate, including the two largest 7.7 and 7.5 events at a worldwide scale.

All earthquakes occurring during the crises and the period 1976-2020 and having a focal mechanism solution (CMTS) have been plotted on Figure 2a.

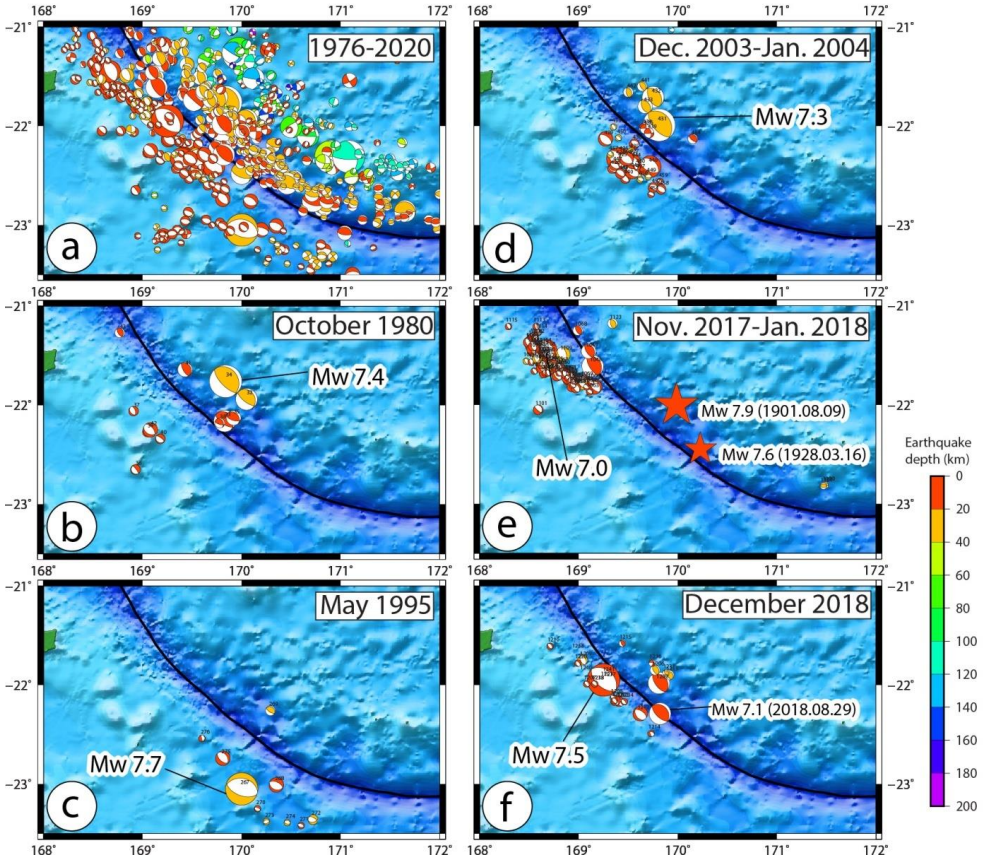

Figure 2: Focal mechanism solutions from CGMT project plotted for the period 1976-2020 with focus on 5 different seismic crises at the Loyalty Ridge-Vanuatu Arc subduction zone.

In October 1980 more than 100 events have been recorded by the worldwide network (Vidale and Kanamori, 1983). The sequence includes twelve M5.4+ events (Figure 2b). Six of them are thrust faulting earthquakes east of the plate boundary (among the two M6.5 + foreshocks and the M7.4 main shock) and five of them are normal faulting earthquakes in the downgoing plate west of the trench. Active sequence began by the three main thrust fault events and followed by the alternance of normal and thrust fault events.

During the May 1995 seismic crisis 13 events with magnitude greater than 5 were located around 23°S, 170°E (Figure 2c). Most of them are normal faulting type southwest of the trench including the M_w 7.7 main shock, 125 km to the southeast of the December 2018 event. This M_w7.7 event is the largest normal faulting earthquake known in the World in a plunging plate on the trench outer slope (Rouland et al., 1995). In detail, this earthquake

https://doi.org/10.5194/nhess-2021-58
Preprint. Discussion started: 18 March 2021
© Author(s) 2021. CC BY 4.0 License.

Natural Hazards and Earth System Sciences
Discussions

and its associated aftershocks are located at the foot of the Loyalty Ridge in the adjacent South Fiji Basin. These normal type events affecting the crust of the South Fiji Basin (from 169.75°E to 171°E) are further far from the axis of the trench relatively to the normal faulting events of the December 2003 and 2018 sequences which are on the Loyalty Ridge (169.5°E). This difference could be explained by a different rheological behavior (more buoyancy of the ridge).

Between December 25, 2003 and January 5, 2004, a shallow seismic swarm very similar to the one of 1980 occurred (same zone, same magnitude and same spatial organization of fault types; Figure 2d) (Régnier et al., 2004). More than 1000 events were recorded by the local IRD seismic network, among which about 270 by the worldwide network including 37 events with magnitude greater than 4.9, 12 with magnitude equal or greater than 6 and two greater than 7. The sequence started with normal faulting events with magnitude up to 6.8 west of the trench, continued by several interplate thrust faulting events including the large M_w7.3 event on December 27 and located immediately to the east of the trench, and terminated by normal faulting events including a large M_w7.1 event on January 3 located again southwest of the trench.

An important seismic crisis occurred from November 2017 to January 2018 with several thousands of events located about 70km-100 km northwest of the December 2018 swarm (Figure 2e). Among them, 350 M4+ events have been recorded and most of the 80 M4.7+ events are normal faulting earthquakes located west of the trench along the northern edge of the Loyalty Ridge. However, in detail, the sequence began by a M_w6.7 and then a M_w5.9 thrust faulting earthquakes on October 31, 2017 and continued by numerous normal faulting foreshocks and the M_w7.0 normal faulting main shock on November 19, 2017.

The December 5, 2018 M_w7.5 earthquake can be considered as part of a seismic crisis that began on August 29, 2018 with a M_w7.1 interplate thrust faulting earthquake located southeastward (Figure 2f). The M_w7.5 normal faulting main event located west of the trench was preceded 4 min. before by a M_w6.3 event (magnitude estimated as 5.8 by the local ORSNET network) and more interestingly was followed 2h25 later by a M_w6.8 interplate thrust faulting east to the trench. During December 2018, about 89, 49 and 18 aftershocks of M 4+, M4.5 and M5+ respectively have been recorded by the local network.

It appears clearly that the successive seismic crises are quite similar and included both interplate thrust fault type earthquakes northeast of the trench and normal fault type events southwest of the trench in the plunging plate (Figure 2). The strong spatiotemporal pattern between these two types of events suggests that static stress interactions may account for triggering non-distant earthquake, normal faulting on the plunging plate triggering interplate thrust faulting or the reverse.

2 The December 5, 2018 earthquake and tsunami

2.1 Earthquake crisis

At 04:18:08 UTC (15:18:08 local time in New Caledonia) on December 5, 2018, a major earthquake (around M_w7.5) occurred 165 km east-south-east of Tadine, Maré, the southernmost inhabited island of the Loyalty Archipelago. Being strongly felt in New Caledonia (Loyalty Islands and the Grande Terre) as far as Nouméa, more than 300 km west from the source (Roger et al., 2019a, 2019b, 2019c), it has been also weakly felt in Port-Vila, capital of Vanuatu, about 470 km to the North according to a CBS News interview of Mr. McGarry, media director at the Vanuatu Daily Post. There is no report of damage linked to the earthquake.

https://doi.org/10.5194/nhess-2021-58
Preprint. Discussion started: 18 March 2021
© Author(s) 2021. CC BY 4.0 License.

Natural Hazards and Earth System Sciences
Discussions

Within minutes, its location and magnitude were determined by the Seismological Observatory of New Caledonia (http://www.seisme.nc, https://bit.ly/2IMkmgM) [M_w7.6, 22.01°S, 169.33°E, 30 km], by USGS [M_w7.5, 21.968°S, 169.446°E, 10 km] and by the Global CMT project (Dziewonski et al., 1981; Ekström et al., 2012) as a quick CMTS [M_w7.5, 21.95°S, 169.25°E]. Maximum distance between these locations is ~15 km, in agreement with the acceptable location errors between the different observatories. The current location of the event is now 21.950°S, 169.427°E, 10 km, 21.95°S, 169.25°E, 17.8 km and 21.969°S, 169.446°E, 12km by USGS, GCMT, and GEOSCOPE respectively.

The seismic moment Mo of this event has been evaluated to 2.49 x 1020 N.m (M_w7.53) by USGS, 2.52 x 1020 N.m by GCMT project, and 2.95 x 1020 N.m (M_w7.58) by the SCARDEC method (GEOSCOPE-IPGP).

The location of the event and the different solutions of its focal mechanism solution indicate that the earthquake is the result of shallow normal faulting along a fault plane trending NW-SE within the plunging Australia Plate on the northern border of the Loyalty Ridge. The proposed parameters for the rupture (strike, dip, rake) are [298°, 43°, -111°], [312°, 36°, -90°] and [297°, 55°, -108°] for USGS, GCMT and GEOSCOPE (SCARDEC) respectively.

Data indicate rupture duration of about 50 s and 3 patches of displacement during the rupture. USGS proposes a fault model (strike 298°, dip 43°) of 160 km x 30 km with a slip ranging up to 3 m mainly distributed in the 10 km upper part of the fault plane (hypocenter being at 12 km) and a maximum displacement patch at an along strike distance around 40 km northward of the hypocenter (https://earthquake.usgs.gov/earthquakes/eventpage/us1000i2gt/finite-fault).

2.2 Tsunami

This earthquake is added to the two local earthquakes reported by the past in the south Vanuatu Subduction zone that triggered major tsunamis in the Loyalty Islands in March 28, 1875 and September 20, 1920 (Sahal et al., 2010) with estimated magnitude of 8.1-8.2 and 7.5-7.8 respectively (Ioualalen et al., 2017), and to the M_w7.7 May 17, 1995 event which occurred close and south to the December 5, 2018 event showing a similar focal mechanism (normal faulting in the plunging plate) as explained hereabove. This event of 1995 was followed by a tsunami that was well observed at the entrance of the first lagoon and on Erakor Island in Port Vila, located south of Efate, Vanuatu (Lardy, 1995).

Considering the strong magnitude of this shallow earthquake, a tsunami alert was released locally by the IRD seismological laboratory to the New Caledonia civil security service (DSCGR) and regionally by the NOAA/PTWC soon after the earthquake occurred. A tsunami was confirmed by real-time tide gauges measurements within minutes at first in the Loyalty Islands, 45 minutes before high tide in Tadine (high tide at 4:30 PM local time and tsunami arrival recorded at 3:43 PM local time) and about one or two minutes after high tide in Hienghène (high tide at 4:25 PM local time and tsunami arrival recorded at 4:26-4:27 PM local time).

2.2.1 Tide gauge records

Tide gauge records used in this study come directly from the pressure sensors (Maré, Ouinné, Thio, Hienghène), from the SHOM Refmar database (Lifou ; http://refmar.shom.fr/en/lifou), from the IOC Sea Level Station Monitoring Network (Lénakel and Port-Vila ; http://www.ioc-sealevelmonitoring.org/) and the ReefTEMPS project (Poindimié ; Varillon et al., 2018). They are visible on Figure 8.

https://doi.org/10.5194/nhess-2021-58
Preprint. Discussion started: 18 March 2021
© Author(s) 2021. CC BY 4.0 License.

Natural Hazards and Earth System Sciences
Discussions

The tide gauge of Maré Island, located in Tadine's Harbor on the southwest coast of this island, was the first to record the tsunami signal at 4:43 UTC (3:43 PM local time – UTC+11), 25 minutes after the shock (Figure 8). Then, the wave train reached the other tide gauges located in New Caledonia (4:43 UTC in Wé, Lifou Is.; 5:11 UTC in Ouinné; 5:10 UTC in Thio; 5:27 UTC in Hienghène) as well as several pressure gauges like in Poindimié, east coast of New Caledonia. According to Roger et al. (2019b) for what concerns New Caledonia only, a maximum tsunami height of ~60-70 cm was recorded by Ouinné tide gauge.

In the Vanuatu, it reached Tanna Island first (4:41 UTC in Lenakel) where it has been recorded by the tide gauge located at Lenakel harbor showing a maximum height of ~1.5 m (amplitude of ~75 cm a.s.l.). In Efate (5:06 UTC in Port-Vila), the tsunami has been also recorded on the tide gauge located at Port Vila where it reached a maximum height of ~50 cm (maximum amplitude of ~25 cm a.s.l.).

Afterwards, it has been also recorded by tide gauges in other locations of the southwestern Pacific region, as far as Port Kembla, Australia, about 2200 km away from the source, North Cape, New Zealand, or Pago Pago in the American Samoa's. Except in New Caledonia and Vanuatu, it never reached more than 30 cm high. Figure 3 locates the different tide gauges that were able to record the tsunami within the southwestern Pacific Region and illustrates the recorded maximum wave height (ITIC communication from Stuart Weinstein, 2018).

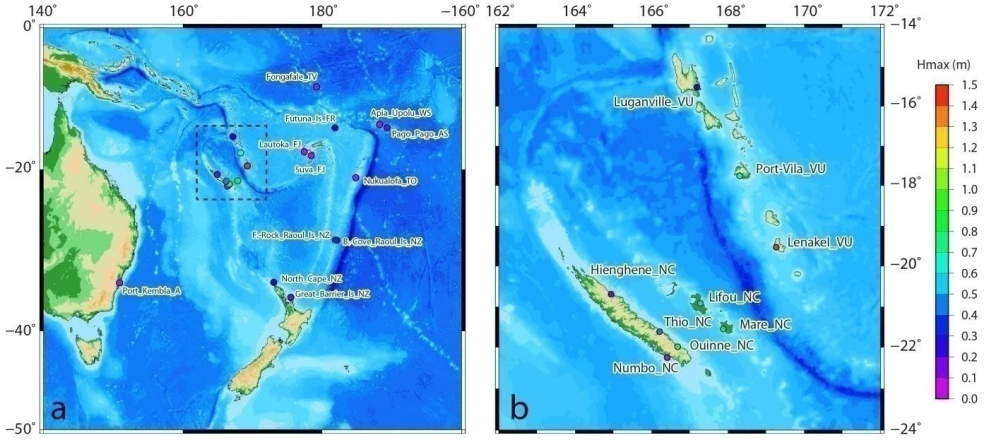

Figure 3: Tsunami maximum wave height recorded on each tide gauge of the southwestern Pacific region.

2.2.2 Eye-witnesses' observations

In the aftermath of this event, two videos have been collected for two different locations: Yaté (Figure 4a), southeast coast of Grande Terre and the Méridien Resort, Isle of Pines, southernmost island of New Caledonia (Figure 4b). The first video from Yaté, circulating on social networks the day of the event, is very informative. It shows the arrival of the tsunami over the fringing reef shelf exposed out of the water by a first important withdrawal of the sea between ~100 and 200 m ; note that the sea was reaching nearly high tide at the moment of the tsunami arrival with a predicted maximum water level of 1.55 m at 4:31 PM local time at Ouinné, the nearby tide gauge, corresponding to a water depth of ~1.2-1.3 m over the reef shelf in Yaté. Two quantitative information come from the video analysis. The first one is an estimate of the tsunami speed from ~ 5 to 10 m.s-

https://doi.org/10.5194/nhess-2021-58
Preprint. Discussion started: 18 March 2021
© Author(s) 2021. CC BY 4.0 License.

Natural Hazards and Earth System Sciences
Discussions

1(18 to 36 km.h-1). The second one is the maximum tsunami height of ~2.3 m reached in ~20 s (after the withdrawal), derived using one isolated mangrove tree exploited as a flood scale afterwards (Figure 4E).

The second video and additional pictures have been provided courtesy of M. Bretault (Technical Director of Méridien Resort of the Isle of Pines). The video shows the tsunami travelling into the shallow channel that encircles the resort complex and its surrounding. (Figure 4B1) With the help of aerial orthophotos (Government of New Caledonia, tile n°55-17-IV, https://georep-dtsi-sgt.opendata.arcgis.com/pages/orthophotographies), one can derive the tsunami speed in the channel of around 5 m.s-1 (18 km.h-1). The pictures have been taken after the tsunami and reveal the damages on several bungalows and around the swimming pool, and show the run-up extent of the waves (Figure 4B2).

In Vanuatu, the tsunami has been reported in several places from Aneityum Island in the south, to Tanna, and Efate Islands. It reached Aneityum first, where the impact has probably been the worse in the whole concerned region by this tsunami, especially in Umetch area where it washed literally the village and plantations with waves reaching ~4 m (Tari and Siba, 2019) and penetrating more than 200 m inland (Vanuatu Daily Post, December 6, 2018) as shown on Figure 4c, leaving people homeless. It has also badly damaged Mystery Island and its airport on the southwest of Aneityum, a major source of incomes for the island. Other places like Anelghowhat have also experienced the tsunami but without important damages as reported in the Vanuatu Daily Post (December 8, 2018). Then it reached Tanna where it has been recorded by Lenakel tide gauge as reported hereabove but it has also been reported by the manager of Ipikel, a village on the southeastern coast of the island, as having reached the first houses without any damages, about 80 m from the shoreline and ~1.5 m high (Isaac, manager of Ipikel, pers. comm., 2019). In Efate, witnesses reported a small inundation on Erakor Island, south of Port Vila (Figure 4d).

https://doi.org/10.5194/nhess-2021-58
Preprint. Discussion started: 18 March 2021
© Author(s) 2021. CC BY 4.0 License.

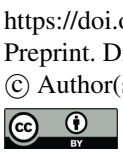

Natural Hazards and Earth System Sciences
Discussions
Open Access
EGU

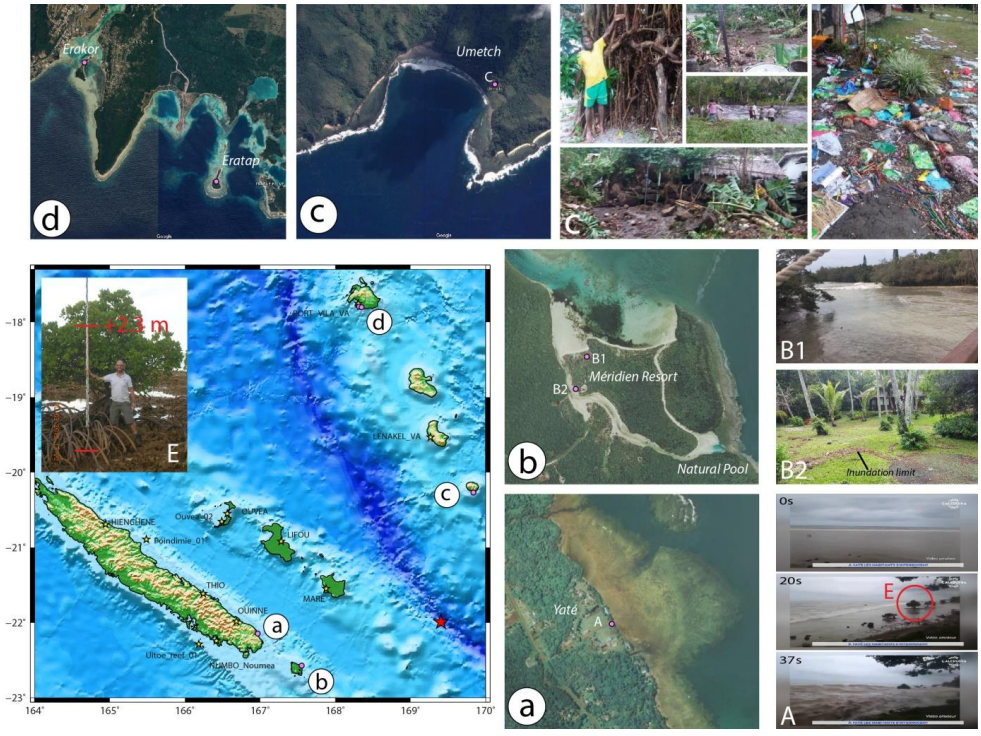

Figure 4: Observations of the tsunami arrival and height in several places in New Caledonia and Vanuatu. a: Yaté; b: Pine Island-Meridien Resort; c: south Aneityum, d: south of Port Vila, south Efate. (Photos credit: a, b: © Georep New Caledonia 2021; c, d: © Google Earth 2021 - CNES/Airbus; A: Caledonia TV; B1 & B2: Moana Bretault; C: Vanuatu Meteorology and Geohazards Department; E: authors).

3 Tsunami modelling

Numerical models are commonly used to assess the tsunami hazard. In this section, a suite of models used to simulate bottom deformation, tsunami generation and propagation and their settings are presented, including details about the Digital Elevation Models (DEM) used in computational grid generation. Tsunami modelling sensitivity to detail the rupture model is presented and finally tsunami simulation results are compared to observations.

3.1 Input data

3.1.1 Bathymetric grids

It is well known that tsunami's behavior is dependent upon the bathymetric features and the coastal geometries (e.g., Matsuyama, 1999; Hentry et al., 2010; Yoon et al., 2014). When it approaches coastlines or seamounts, the wave shoaling leads to the rising-up of the amplitude and slows down the tsunami as the water depth reduces. It is even worse when the tsunami enters harbors, bays, lagoons or fjords able to produce resonance, a phenomenon

https://doi.org/10.5194/nhess-2021-58
Preprint. Discussion started: 18 March 2021
© Author(s) 2021. CC BY 4.0 License.


particularly well studied during the two last decades (e.g., Barua et al., 2006; Rabinovich, 2009; Roger et al., 2010; Roeber et al., 2010; Bellotti et al., 2012; Vela et al., 2014; Aranguiz et al., 2019). It is also possible that a resonant behavior occurs between neighboring islands like it happened in Hawaii during the 2006 Kuril tsunami (Munger and Cheung, 2008).

For these reasons, it is necessary to model tsunami propagation on bathymetric grids keeping the most relevant details. There are two main traditional downscaling strategies in wave and tsunami modelling. One uses a sequence of nested structured-grid models; the other relies on a single unstructured-grid model. Both techniques aim at obtaining high-resolution wave fields in shallow area and provide similar results (Harig et al., 2008 ; Pallares et al., 2016), even if several studies have highlighted that the use of only one unstructured mesh grid for tsunami modelling provides better reproduction of tsunami observations and records in comparison to nested grids scheme use (e.g. Harig et al., 2008; Shigihara and Fujima, 2012). When considering the presence of many archipelagos forming the Melanesian volcanic arc (Solomon Islands and Vanuatu, Figure 3) and peculiar details along the New-Caledonia's coastline (Figures 4), the unstructured grid method provides multiple advantages. This technique allows more flexibility in mesh design and can capture more coastline details than regular meshes at the same computational cost.

In this study, bathymetric grids have been built using: 1) Smith and Sandwell (1997) v. 8.2 dataset, 2) an extended ~180 m resolution DEM covering the whole economic zone of New Caledonia and Vanuatu produced especially for the assessment of tsunami hazard in New Caledonia and 3) 10 m resolution data on harbors where tide gauges and/or witnesses' observations are located. These latest data are coming from digitized nautical charts, aerial pictures interpretation and multibeam bathymetric surveys. The first grid consists of a 7 km resolution regular grid covering the source area and it is mainly used to model the bottom deformation using the Okada's fault plane model (Okada, 1985). The second one is an unstructured mesh forming a triangular irregular network (TIN) DEM (Figure 5a, b and c) with varying mesh size (from 5 m along the coastline to 2150 m in the deep ocean, with a median value of 70 m, corresponding to the target size for grid resolution along the coastline) and is used for calculation of tsunami generation, propagation and interaction with the shallow water features.

The TIN DEM generation has been made with Shingle 2.0 (Candy and Pietrzak, 2018), an automatic grid generation algorithm. A variable mesh size function is designed to capture the evolution of the tsunami wave with a spatial discretization of 30 points per wavelength. Along the coastline or places with shallow features and gauge stations, additional mesh refinement rules are imposed in the mesh size function. Figure 5b and c show the increase of spatial resolution when approaching the barrier reef and the coastline.

https://doi.org/10.5194/nhess-2021-58
Preprint. Discussion started: 18 March 2021
© Author(s) 2021. CC BY 4.0 License.

Natural Hazards and Earth System Sciences
Discussions

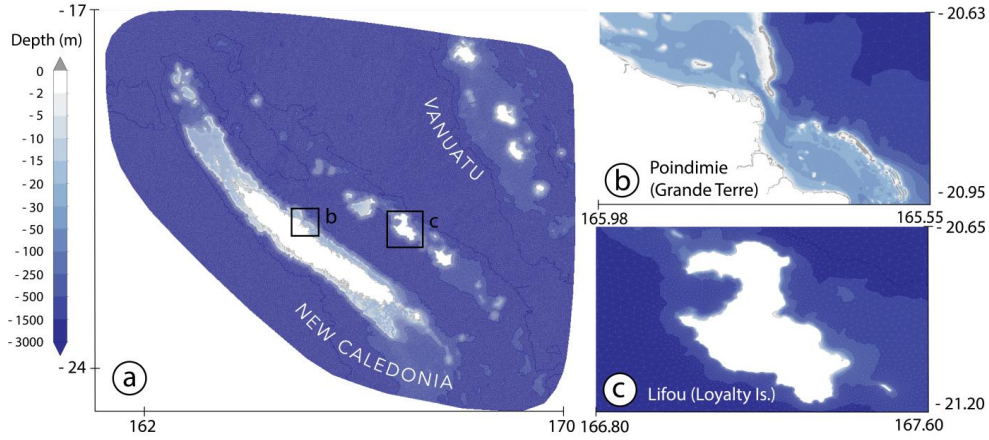

Figure 5: Triangular irregular network (TIN) DEM including New Caledonia and South Vanuatu Islands.

3.1.2 Earthquake parameters

Most of tsunami modelling codes are using Okada (1985)'s surface deformation expressions related to an earthquake rupture. The calculation of this deformation is directly linked to crucial parameters like the depth of the hypocenter and the movement on the fault plane.

Several locations of the hypocenter as well as magnitudes and focal mechanism solutions for the December 5, 2018 earthquake have been proposed by the different observatories (USGS, GCMT, IPGP/SCARDEC). However, there are quite similar: a M_w 7.5 to 7.6 normal fault-type event along the northern border of the Loyalty ridge entering the subduction zone. Considering the geological and tectonic context and the effects of the tsunami along the shores of New Caledonia, the parameters the authors have decided to use for this study are issued from the GCMT catalog: latitude -21.95°S, longitude 169.25°E, depth 17 km, strike of the ruptured fault plane 312°, dip 36° and rake -90°.

Taking a rupture length L of 80 km, a rupture width W of 30 km, (a surface A of 2400 km²), a M_o of 2.52 e+20 N-m and a rigidity (or shear) modulus μ of 3 x 10^{11} dyne cm-2, the relationship $s = \frac{M_0}{\mu A}$ gives the coseismic slip on the fault plane s = 3.5 m. A uniform slip distribution along the fault plane is considered in the modelling exercise.

3.2 Numerical modelling strategy

3.2.1. Seafloor deformation calculation

The seafloor deformation is derived using the Okada (1985)'s fault plane model implemented in the bottom deformation module of MOST (Method Of Splitting Tsunami, Titov and Synolakis 1995, 1996, 1997). Different fault-plane parameters are tested with this module onto the 7 km computational grid to provide Okada's static solutions noted b0 hereafter. Then, these bottom motion solutions are added to the TIN DEM for further tsunami simulations.

https://doi.org/10.5194/nhess-2021-58
Preprint. Discussion started: 18 March 2021
© Author(s) 2021. CC BY 4.0 License.

Natural Hazards and Earth System Sciences
Discussions

3.2.2. Tsunami generation and propagation modelling

Tsunami waves generated by the moving seafloor and their propagation are computed using the Semi-implicit Cross-scale Hydroscience Integrated System Model (SCHISM), an unstructured ocean model developed by the Virginia Institute of Marine Science (Zhang et al. 2015, 2016a) based on the former 3D ocean model SELFE from Zhang and Baptista (2008). It is an open-source community-supported ocean model heavily tested and under continuous improvement in laboratories worldwide, oriented towards a handful of different modelling domains using specific modules like wind-wave modelling (e.g. Roland et al., 2012; Hsiao et al., 2020), sediment transport modelling (e.g. Pinto et al., 2012; Lopez and Baptista, 2017) or tsunami modelling (e.g. Zhang et al., 2016b; Priest and Allan, 2019). Modelling of tsunami propagation and coastal interaction is performed through unstructured grids like TIN. Inundation could also be calculated but the authors have decided not to do it due to the bad quality of topographic data. According to Horrillo et al. (2015), SCHISM has passed successfully the United States of America NTHMP (National Tsunami Hazard Mitigation Program) benchmarks from the OAR-PMEL-135 standard providing a list of problems like the famous 1993 Okushiri tsunami exercise (https://nctr.pmel.noaa.gov/benchmark/index.html).

SCHISM is capable of solving the 3-D Reynolds-Averaged Navier-Stokes (RANS) equations. It uses a semi-implicit Galerkin finite-element and finite-volume method on unstructured grids (Zhang and Baptista, 2008; Zhang et al., 2016a, 2016b) with time stepping with no CFL (Courant-Friedrich-Lewy) stability/convergence condition. This way, large time steps could be applied even with high resolution meshes. In this study, SCHISM is used in barotropic mode with hydrostatic assumption and only one layer. In 2-D mode, RANS equations are depth-integrated, and the circulation is described using Non-linear Shallow-water Wave equations (NSW), a simplification widely used to model tsunamis. Neglecting wind stress, earth tidal potential and atmospheric pressure forces, the NSW equations used in SCHISM 2-D at point (x,y) with depth h below the geoid are :

Continuity equation: $\frac{\partial(\eta - b)}{\partial t} + \nabla.(uH) = 0$

Momentum equation: $\frac{\partial u}{\partial t} + (u.\nabla)u = f(v, -u) - g\nabla\eta - f_{hd} - \frac{\tau_b}{H}$

Here, t is time, u(x,y,t) the depth averaged horizontal velocity with components (u,v), η the sea surface elevation above the geoid, b the seabed displacement (positive for uplift), H the total water depth (H=η-b+h), f the Coriolis factor, g the gravity acceleration, f_{hd} the horizontal eddy viscosity (set to 10^{-4} $m^2.s^{-1}$) and τ_b the bottom drag following a quadratic form:

$$\tau_b = g\frac{{M_n}^2}{H^{1/3}}\|u\|u$$

where M_n is Manning's roughness coefficient set spatially uniform with a value of 0.025 $s.m^{-1/3}$. All tsunami simulations were performed assuming that prevailing tide was static (no flow) and equal to high water (+1.6m). To limit undesirable wave reflection, a Flather radiation condition (Flather, 1987) is applied along the open boundaries with specified outer values 0 $m.s^{-1}$ and 1.6 m for U and η respectively.

https://doi.org/10.5194/nhess-2021-58
Preprint. Discussion started: 18 March 2021
© Author(s) 2021. CC BY 4.0 License.

Natural Hazards and Earth System Sciences
Discussions

In a first step, SCHISM is used to generate the sea-surface initial deformation and flow dynamics in response to the bottom motion. The dynamic displacement of the seafloor can be described in SCHISM by adding a time dependent seafloor displacement term *b* incorporated in NSW governing equations. This is done by multiplying Okada's static solution b_0 by a uniform rate function of the rising time. In agreement with seismic records, we used 50 s for the rising time and ran SCHISM with a time stepping dt = 1 s. During the rising time, the seafloor anomaly b_0 is progressively injected to give the initial condition for the free surface and horizontal momentum conditions. Then, to simulate tsunami propagation, the model runs with dt = 30 s for a duration of 3 hours. It is worth noting that using the default value of 10 s for the rising time, like done by many authors, give marginal effects on results.

To detect changes due to fault parameters, total wave energy (*E*, unit j.m-2) is added in SCHISM outputs, as the sum of two components, kinetic energy (first term) and gravitational potential energy (second term):

$$E = \frac{1}{2}\rho H U^2 + \frac{1}{2}\rho g \eta^2$$

It is again important to underline that the sea-level has been set to a high tide value of 1.6 m, which corresponds to the situation when the tsunami reached New Caledonia on December 5, 2018.

3.3 Simulation results

Figure 6 presents the maximum wave energy map obtained after 3 hours of tsunami propagation over the TIN DEM. It highlights the important role played by the strike angle of the fault plane. This parameter should absolutely be chosen accurately in good agreement with the geology. A 298° (USGS) and a 312° (GCMT) strike will lead to a different behavior of the tsunami, focusing its main energy path generally perpendicularly to the strike of the fault plane with respect to the slip angle (=rake) (Okal, 1988). But if the waves encounter submarine features like seamounts or ridges, the trajectory of the tsunami could be dramatically modified as these features act as wave guides, focusing the wave train in another direction due to the fact that the tsunami speed relies only on the bathymetric depth in the open ocean (Satake, 1988; Titov et al., 2005; Swapna and Srivastava, 2014). That is exactly what happens in the presented case: the 312° strike proposed from the CGMT observatory sends larger wave energy towards the south of New Caledonia (Isle of Pines) than the 298° strike from USGS. Along the east coast of the Isle of Pines, the increase in energy is in the range 20% to 30% and up to 50% near specific coastal features like bay entrances (15 to 25 $kJ.m^{-2}$ there with CGMT settings). Along the south coast of Aneityum, the only observation site located in the main energy path of the tsunami, the total wave energy decreases by about 10%. (20 to 30 $kJ.m^{-2}$ there with CGMT settings). Naturally, the choice to keep the CGMT solution allows to keep maximum energy toward the Isle of Pines without reducing drastically the energy sent toward Aneityum.

https://doi.org/10.5194/nhess-2021-58
Preprint. Discussion started: 18 March 2021
© Author(s) 2021. CC BY 4.0 License.

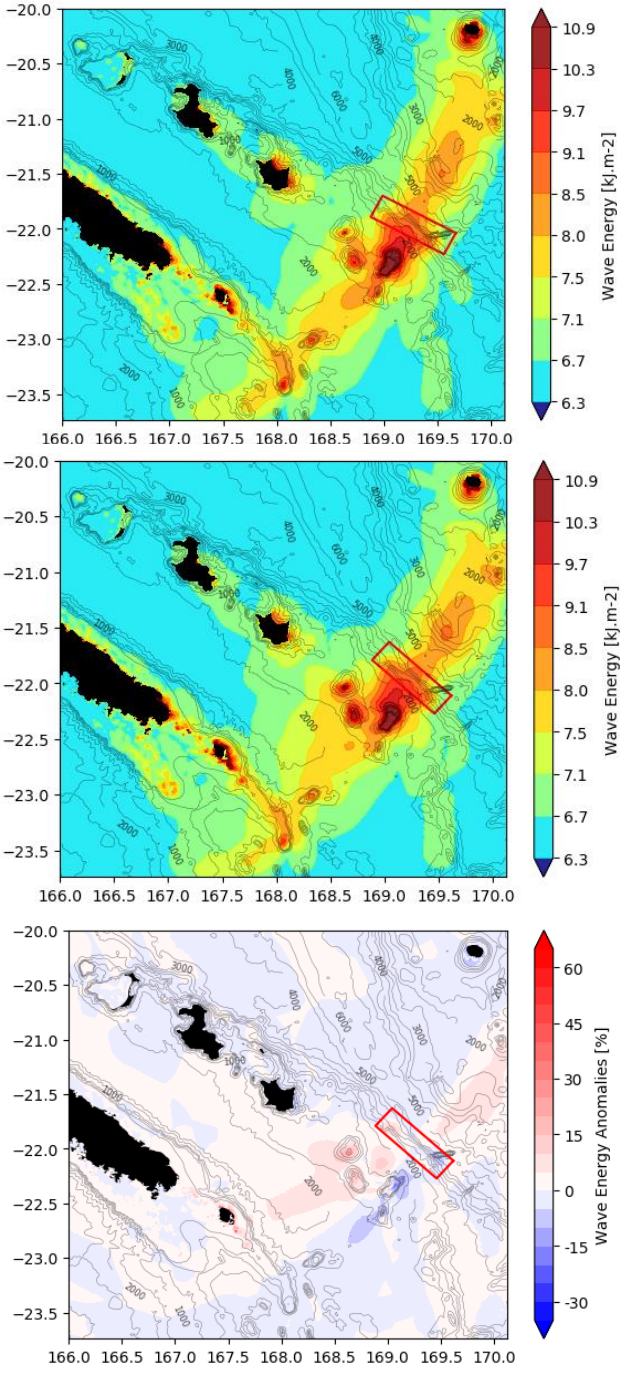

https://doi.org/10.5194/nhess-2021-58
Preprint. Discussion started: 18 March 2021
© Author(s) 2021. CC BY 4.0 License.

Figure 6: Total wave energy E maps for two different strikes: 298° (top, USGS settings) and 312° (center, GCMT settings) and relative E anomaly between the two (bottom). The bathymetric contours underline the features able to influence the wave propagation.

Thus, the following results have been obtained using a strike set to 312° (GCMT solution).

The tsunami energy is partially captured by the submarine ridges oriented perpendicular to its main propagation way, leading to amplifications in the Loyalty Islands (via the Loyalty Ridge) and around the Isle of Pines (via the south-eastern seamounts complex of the Pines Ridge). The TIN DEM allows zooming onto specific areas like Aneityum (Figure 7b), the Isle of Pines (Figure 7c), Yaté (Figure 7d) and Port-Vila (Figure 7e) helping to further compare the testimonials to the modelling results. There is important coastal amplification of the tsunami along the south coast of Aneityum from Anelghowhat to Umetch (Figure 4c), showing maximum wave amplitude of more than 1.5 m between Mystery Island and the main island (Figure 7b). Coastal amplification is also relatively important in some restricted locations along the east coast of the Isle of Pines (Figure 7c) showing wave amplitude of more than 1 m in front of the Meridian Resort but also ~ 40-50 cm in the bay of Ouameo on the west coast. Wave amplification along the coast of Yaté (south-eastern part of Grande Terre, Figure 7d) leads to maximum wave amplitude of ~50 cm in front of the church of Touaourou and in the Yaté River estuary. Finally, focus on Port-Vila, located along the south coast of Efate Island (Figure 7e) and on Sulphur bay, southeast of Tanna Island, show wave amplification in a few places, reaching ~40 cm maximum in both cases.

https://doi.org/10.5194/nhess-2021-58
Preprint. Discussion started: 18 March 2021
© Author(s) 2021. CC BY 4.0 License.

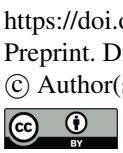

Natural Hazards and Earth System Sciences
Discussions
Open Access
EGU

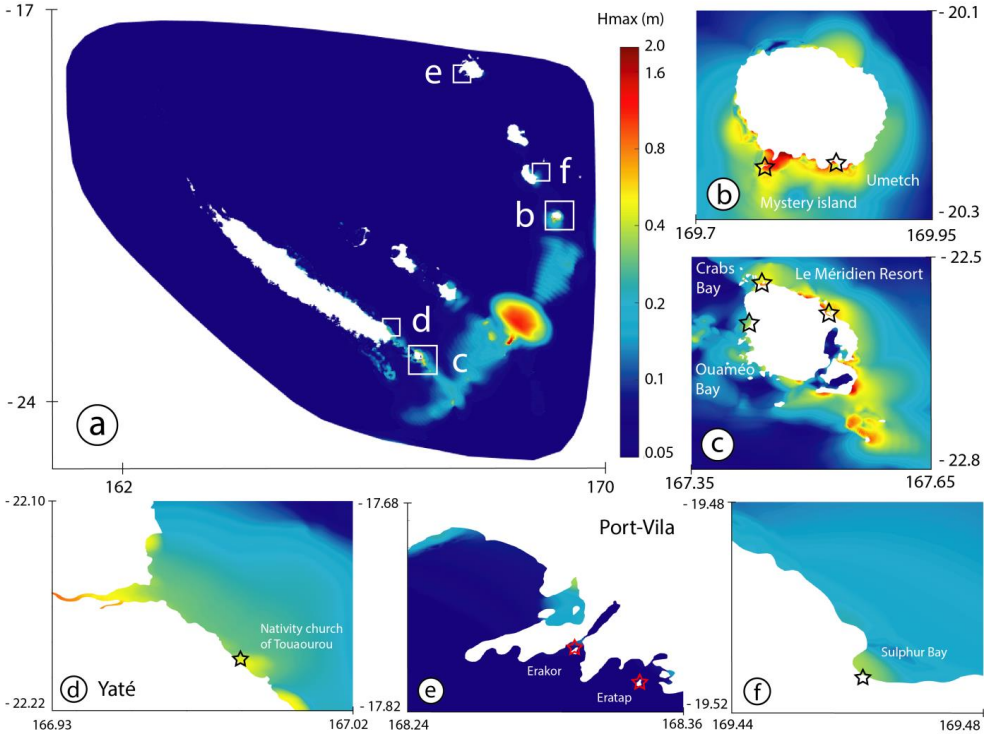

Figure 7: Maximum wave height maps obtained after 3 hours of tsunami propagation on the TIN DEM for the December 5, 2018 event in New Caledonia and South Vanuatu. a: for the entire area, b: Aneityum island, c: Isle of Pines, d: Yaté; e: Port vila, Efate; f: Sulphur Bay, Tanna. Stars stand for eye-witnesses observation points.

Tide gauge simulation results are compared to real maregraphic records on Figure 8. For Maré, Ouinné, Thio and Hienghène, the data shown are coming directly from the raw dataset of the pressure sensors. For Lifou, the data have been provided by the SHOM (http://refmar.shom.fr/en/lifou). The data shown for Lenakel and Port-Vila are coming from the IOC database (www.ioc-sealevelmonitoring.org/) and the data from Poindimié are coming from a local New Caledonia coastal water monitoring project (ReefTEMPS project: http://www.reeftemps.science/en/data/).

At Tadine, Maré, the modelling is not able to reproduce correctly the tide gauge record in terms of arrival time and wave amplitude (Figure 8a). It shows a delay of ~5 min, the modelling being faster than the reality. Also, it does not reproduce the oscillation of period ~4-5 min with amplitudes more than three times those that are modeled.

At Wé (Lifou), the simulated signal exhibits some strong similarities with the real one recorded in terms of polarity, wave amplitude and periodicity, but there is a delay of more than 5 minutes, the modelling being faster than the reality (Figure 8b).

At Thio, the modelling is able to reproduce the real record for what concerns the polarity, the amplitude or the periodicity but not exactly the arrival time, being still early of a couple of minutes (Figure 8c).

https://doi.org/10.5194/nhess-2021-58
Preprint. Discussion started: 18 March 2021
© Author(s) 2021. CC BY 4.0 License.


At Ouinné, the modelling is not able to reproduce the recorded signal, except for the first wave polarity, showing a strong delay of nearly 5 min, the modelling being the fastest (Figure 8d). An oscillation with a period of ~6-8 min seems to occur after the first arrival.

At Poindimié - Passe de la Fourmi, there is a good agreement between the modelling and the reality: the arrival time only exhibits a small delay of 1-2 min, the modelled signal being the fastest (Figure 8e). The wave amplitude and polarity are quite good, and the periodicity shows only a few differences that will be discussed further.

At Hienghène, there are differences in arrival time (~2-3 min) between the modelled and the real tide gauge records, the modelled one being the fastest (Figure 8f). The wave polarity and periodicity are well reproduced but the amplitude is slightly overestimated by the modelling.

In Vanatu, at Lenakel, Tanna, there is good agreement between the arrival time and first wave amplitude of the modelled and real tsunami signal (Figure 8g). But the periodicity and amplitudes are strongly different, the modelling being unable to reproduce what looks like a resonant oscillation with a period of ~6 min and a maximum amplitude reaching nearly 40 cm around 25 min after the first tsunami wave arrival.

At Port-Vila the simulated signal well reproduces the tide gauge record in terms of arrival time ~40 min after the earthquake (exhibiting only a small delay of ~1-2 min), but also in terms of polarity, wave amplitudes and periodicity (Figure 8h). Note that the biggest through and peak occurring after 100 min are not sufficiently high in the simulation.

https://doi.org/10.5194/nhess-2021-58
Preprint. Discussion started: 18 March 2021
© Author(s) 2021. CC BY 4.0 License.

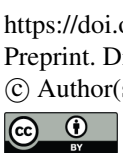

Natural Hazards and Earth System Sciences
Discussions
Open Access
EGU

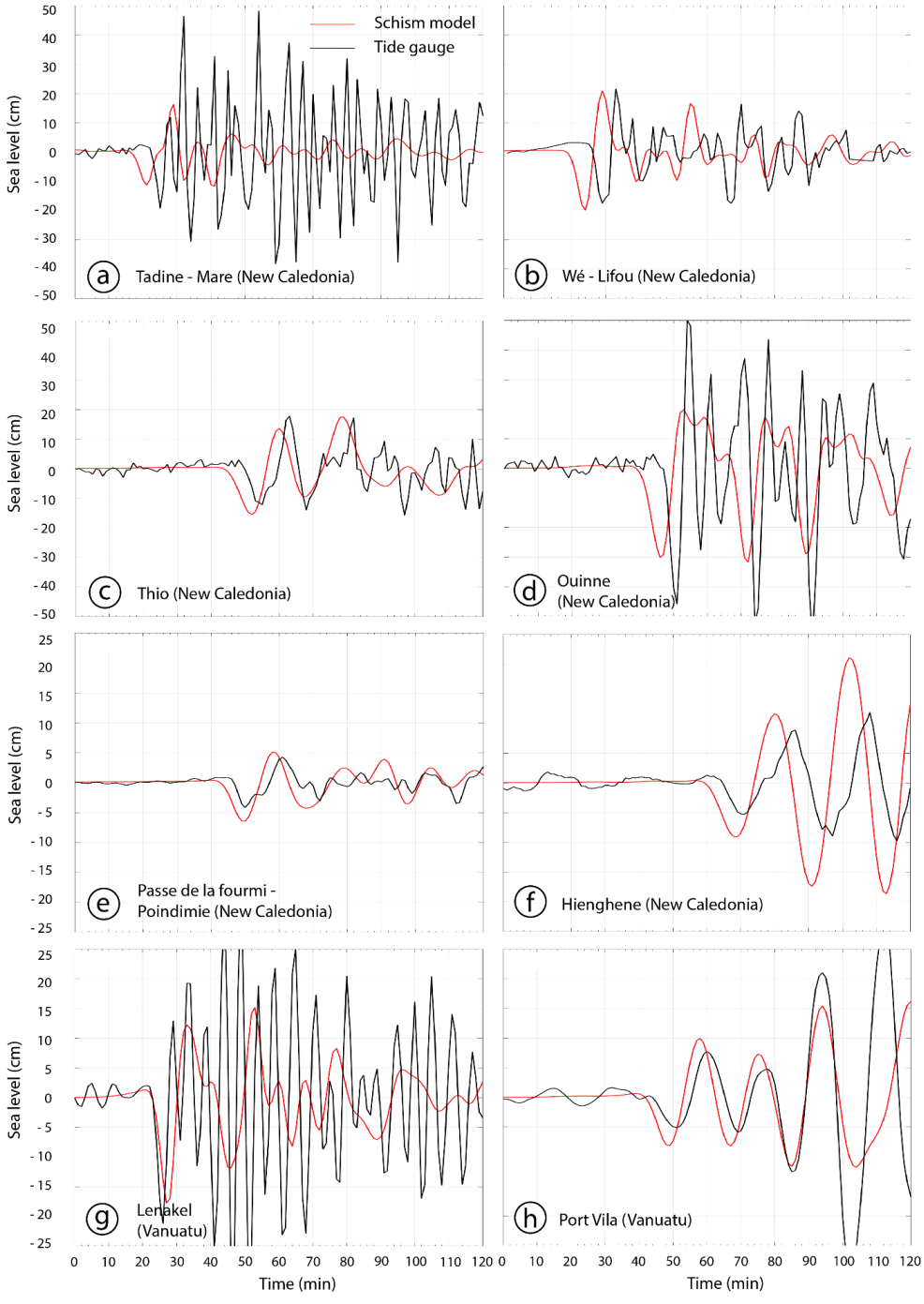

Figure 8: Comparison between real (black) and simulated (red) records for 8 different tide gauges located in New Caledonia (a, b, c, d, e, f) and Vanuatu (g, h). These tide gauges are located on figure 3b. Time is related to the earthquake occurrence time (4:18 UTC). Be careful to the sea level scale for each figure.

425

https://doi.org/10.5194/nhess-2021-58
Preprint. Discussion started: 18 March 2021
© Author(s) 2021. CC BY 4.0 License.

Natural Hazards and Earth System Sciences
Discussions

4 Discussion

The comparison of the maximum energy path of the tsunami as a function of strike on the energy maps shown on Figure 6 highlights the fact that a 312° angle has a slightly bigger impact on the Isle of Pines matching much better with the observations than a 298° angle. The maximum wave height map calculated over a high-resolution TIN grid (Figure 7) clearly indicates that the modelling results are in good agreement with the direct observations of the tsunami in both New Caledonia and Vanuatu on December 5, 2018. In fact, the coastal places where the modelling shows maximum amplitudes (> 0.4-0.5 m) are also the places where witnesses reported the tsunami (Isle of Pines, Aneityum, Yaté, Tanna, Erakor Island) and sometimes damages (Isle of Pines-Meridien resort, Aneityum, Mystery Island and southern coast to Umetch.

In addition, the tide gauge record comparisons show that globally the chosen seismic parameters and therefore, tsunami generation and propagation model, are together able to reproduce the tsunami records, in terms of arrival times (Figures 8e, g & h) especially in far-field location (Poindimié, Tanna and Port-Vila tide gauges), polarity (Figures 8b, d, e, f, g & h), and amplitude (Figures 8b, e & h).

Except for Poindimié-Passe de la Fourmi where there is pressure sensor offshore the reef barrier, the observed delay between the simulations and the reality (the modelled signal being always the fastest) on all the New Caledonia coastal tide gauges managed by the SHOM (hydrographic service of the French navy) is explained by the fact that there are some transmission issues from the gauge to the datacenter.

Concerning the high frequency oscillations that the modelling is not able to reproduce, especially at Maré, Ouinné and Lenakel, it is presumably the result of resonant behavior of the tsunami waves interacting with semi-enclosed water bodies represented by Maré Harbor, Ouinné Harbor and Lenakel's Bay, and fringing reef as well explained for other places in the literature (e.g. Horillo et al., 2008; Rabinovich, 2009; Aranguiz, 2015). The fact that the high-resolution coastal zones surrounding the location of the tide gauges have been built from sparse bathymetric data coming from low resolution nautical charts and aerial pictures interpretation could explain that the modelling is not able to reproduce the resonance as the shape of the water bodies, and thus their natural oscillation modes are not exactly the same. According to previous studies, it is a safe bet that either a source refinement (complex source showing slip heterogeneity for example) or high-resolution bathymetric data coming from multibeam or LIDAR surveys would be able to reproduce such phenomenon in these small and complicated places (e.g. Sahal et al., 2009; Vela et al., 2014).

Considering both maximum amplitude maps compared to the testimonials (locations and amplitudes) and the tide gauges simulation results comparison to the real recorded data, the simple fault plane rupture scenario chosen for this study provides quite good results.

It is interesting to notice that, nearly two years after the tsunami occurred, hidden observations are still transmitted by witnesses. Tsunami modelling showing that the west coast of the Isle of Pines would have also been impacted by the tsunami, we questioned the diving center and the Kodjeu Hotel located within the Ouaméo bay: the final testimony is that the diving club boat, supposed to be load at high tide, was laying on the sand instead at the exact arrival time of the tsunami (P.-E. Faivre, pers. comm., 2020). Then the water came back and the sea rose above its natural maximum (according to a local fisherman, 2019).

https://doi.org/10.5194/nhess-2021-58
Preprint. Discussion started: 18 March 2021
© Author(s) 2021. CC BY 4.0 License.


5 Conclusions

The modelling results presented in this paper and dealing with the December 5, 2018 South Vanuatu tsunami indicate that using a simple fault plane rupture scenario is enough in such case of near field event to reproduce the tsunami correctly with a hazard management point of view. In fact, the study of this local event helps to assess the accuracy of tsunami modelling with MOST and SCHISM models and also, the quality of the DEM used, especially the TIN DEM. Coupled with the study of other historical tsunamis (regional and ocean scales) also recorded on New Caledonia tide gauges, it represents the basement of the building of a scenario database, with tsunami sources located all around the Pacific Ocean ring of fire.

As study perspectives, it would be interesting to look at the tsunami effects at low tide to compare to other similar events in terms of amplitude/periodicity that have absolutely not been perceived by the coastal population. The role played by the tide in tsunami impact has been demonstrated by several studies (e.g. Ford et al., 2014). Also, such small amplitude event occurring at low tide could have been dramatic as lots of people are looking for shells and octopuses on the fringing reef. Finally, new modellings at high tide considering the sea-level rise due to global warming would help to assess the future impact of such small tsunami over island communities with a question that arises: would the growth of coastal ecosystems such as corals and mangroves be able to adapt quickly enough to rising sea level to maintain their protective role against small events?

Acknowledgements

The authors are very grateful to the Vanuatu Meteorology and Geohazards Department which provided the post tsunami survey report about Aneityum, and to all the people having shared their testimony of the December 5, 2018 tsunami collected within the months following the event, but also more specifically during the 2019 PALEOTSU field survey of paleotsunami deposits all around New Caledonia. They are also very grateful with Christopher Moore (NOAA) who provided support for the use of MOST and to Paul Wessel and Walter Smith who developed and maintain the free GMT mapping tools which was used to produced most of the maps of this study. This study has been done within and funded by the TSUCAL project.

Authors' contribution:

JR: study supervision; field investigations; DEM construction; MOST modelling; writing; figures preparation.
BP: study supervision; field investigations; writing; figures preparation.
MD: unstructured grid construction; data processing; figures preparation.
JL: MOST & SCHISM modelling; writing; figures preparation.
JA: funding acquisition; data processing; results discussion.
PL: seismic data processing.
BT: mapping; data processing.
CB: seismic network maintenance.
DV: seismic network maintenance.

https://doi.org/10.5194/nhess-2021-58
Preprint. Discussion started: 18 March 2021
© Author(s) 2021. CC BY 4.0 License.

Natural Hazards and Earth System Sciences
Discussions

References

Aranguiz, R.: Tsunami resonance in the Bay of Conception (Chile) and the effect of future events, Engineers and Planners, 93-113, https://doi.org/10.1016/B978-0-12-801060-0.00006-X, 2015.

Aranguiz, R., Catalan, P.A., Cecioni, C., Bellotti, G., Henriquez, P. and Gonzalez, J.: Tsunami resonance and spatial pattern of natural oscillation modes with multiple resonators, Journal of Geophysical Research, Oceans, 124(11), https://doi.org/10.1029/2019JC015206, 2019.

Bellotti, G., Briganti, R. and Beltrami, G.M.: The combined role of bay and shelf modes in tsunami amplification along the coast, Journal of Geophysical Research, Oceans, 117(C8), https://doi.org/10.1029/2012JC008061, 2012.

Barua, D.K., Allyn, N.F. and Quick, M.C.: Modelling tsunami and resonance response of Alberni Inlet, British Columbia, Coastal Engineering, 1590-1602, https://doi.org/10.1142/9789812709554_0135, 2006.

Båth, M.: Earthquake energy and magnitude, Physics and Chemistry of the Earth, 7, 115-165, https://doi.org/10.1016/0079-1946(66)90003-6, 1966.

Calmant S., Pelletier B., Bevis M., Taylor F., Lebellegard P., and Phillips, D.: New insights on the tectonics of the New Hebrides subduction zone based on GPS results, J. Geophys. Res., 108, B6, 2319-2340, 2003.

Candy, A. S. and Pietrzak, J. D.: Shingle 2.0: generalising self-consistent and automated domain discretisation for multi-scale geophysical models, Geosci. Model Dev., 11, 213–234, https://doi.org/10.5194/gmd-11-213-2018, 2018.

Daniel J., Collot J.Y., Monzier M., Pelletier B., Butscher J., Deplus C., Dubois J., Gerard M., Maillet P., Monjaret M.C., Recy J., Renard V., Rigolot P. and Temakon S.J. : Subduction et collision le long de l'arc des Nouvelles-Hébrides (Vanuatu) : résultats préliminaires de la campagne SEAPSO (leg I). C.R. Acad. Sci. Paris, t. 303, série II, n° 9, pp. 805-810, 1986.

Dziewonski, A.M., Chou, T.-A. and Woodhouse, J.H.: Determination of earthquake source parameters from waveform data for studies of global and regional seismicity, Journal of Geophysical Research, 86, 2825-2852, https://doi.org/10.1029/JB086iB04p02825, 1981.

Ekström, G., Nettles, M. and Dziewonski, A.M.: The global CMT project 2004-2010: Centroid-moment tensors for 13,017 earthquakes, Phys of the Earth and Planetary Interiors, 200-201, 1-9, https://doi.org/10.1016/j.pepi.2012.04.002, 2012.

Flather, R.A.: A tidal model of Northeast Pacific, Atmosphere–Ocean, 25, 22-45, 1987.

Ford, M., Becker, J.M., Merrifield, M.A. and Song, T.: Marshall Islands fringing reef and atoll lagoon observations of the Tohoku tsunami. Pure and Applied Geophysics, 171, 3351-3363, https://doi.org/10.1007/s00024-013-0757-8, 2014.

Harig, S., Chaeroni, Pranowo, W.S. and Behrens, J.: Tsunami simulations on several scales. Ocean Dynamics, 58, 429-440, 2008.

https://doi.org/10.5194/nhess-2021-58
Preprint. Discussion started: 18 March 2021
© Author(s) 2021. CC BY 4.0 License.

Hentry, C., Chandrasekar, N., Saravanan, S. and DajkumarSahayam, J.: Influence of geomorphology and bathymetry on the effects of the 2004 tsunami at Colachel, South India, Bulletin of Engineering Geology and the Environment, 69, 431-442, https://doi.org/10.1007/s10064-010-0303-1, 2010.

Horrillo, J., Grilli, S.T., Nicolsky, D., Roeber, V. and Zhang, J.: Performance benchmarking tsunami models for NTHMP's inundation mapping activities, Pure and Applied Geophysics, 172, 869-884, http://doi.org/10.1007/s00024-014-0891-y, 2015.

Horrillo, J., Knight, W. and Kowalik, Z.: 2008 Kuril Islands tsunami of November 2006: 2. Impact at Crescent City by local enhancement, Journal of Geophysical Research: Oceans, 113(C1), https://doi.org/10.1029/2007JC004404, 2008.

Hsiao, S.-C., Chen, H., Wu, H.-L., Chen, W.-B., Chang, C.-H., Gui, W.-D., Chen, H.-M. and Lin, L.-H.: Numerical simulation of large wave heights from super typhoon Nepartak (2016) in the eastern waters of Taiwan, Journal of Marine Science and Engineering, 8(3), 217, https://doi.org/10.3390/jmse8030217, 2020.

Ioualalen, M., Pelletier, B., and Solis Gordillo, G.: Investigating the March 28th 1875 and the September 20th 1920 earthquakes/tsunamis of the Southern Vanuatu arc, offshore Loyalty Islands, New Caledonia, Tectonophysics, 709, 20-38, https://doi.org/10.1016/j.tecto.2017.05.006, 2017.

Lardy M. : Quelques remarques à propos du séisme et du tsunami du 17 mai 1995 à Port Vila, Note ORSTOM (ex IRD). May 29, 1995.

Lopez, J.E. and Baptista, M.A.: Benchmarking an unstructured grid sediment model in an energetic estuary. Ocean Modelling, 110, 32-48, https://doi.org/10.1016/j.ocemod.2016.12.006, 2017.

Louat, R., and Pelletier, B.: Seismotectonics and present-day relative plate motions in the New Hebrides - North Fiji basin region, Tectonophysics, v.167, p. 41-55, 1989.

Matsuyama, M.: The effect of bathymetry on tsunami characteristics at Sisano Lagoon, Papua New Guinea, Geophysical Research Letters, 26(23), 3513-3516, https://doi.org/10.1029/1999GL005412, 1999.

Maillet, P., Monzier, M., Eissen, J.P. and Louat, R.: Geodynamics of an arc ridge junction: the case of the New Hebrides arc-North Fiji Basin. Tectonophysics,165, 251-268, 1989.

Monzier, M., Maillet, P., Foyo Herrera, J., Louat, R., Missegue, F. and Pontoise, B.: The termination of the southern New Hebrides subduction zone (southwestern Pacific), Tectonophysics, 101,177-184, 1984.

Monzier, M., Boulin, J., Collot, J.Y., Daniel, J., Lallemand, S. and Pelletier, B.: Premiers résultats des plongées NAUTILE de la campagne SUPSO 1 sur la zone de collision "ride des Loyauté/arc des Nouvelles-Hébrides" (sud-ouest Pacifique), C.R. Acad. Sci. Paris, t. 309, série II, p. 2069-2076, 1989.

Monzier, M., Daniel, J. and Maillet, P.: La collision « ride des Loyauté/arc des Nouvelles Hébrides » (Pacifique Sud-Ouest), Oceanol. Acta, 10, 43-56, 1990.

Monzier M.: Un modèle de collision arc insulaire-ride océanique. Evolution sismo-tectonique et petrologie des volcanites de la zone d'affrontement arc des Nouvelles-Hébrides - ride des Loyauté, Thèse de doctorat, Univ. Française du Pacifique, Nouméa. 2 volumes, 322 p., 1993.

https://doi.org/10.5194/nhess-2021-58
Preprint. Discussion started: 18 March 2021
© Author(s) 2021. CC BY 4.0 License.

Natural Hazards and Earth System Sciences Discussions

Munger, S. and Cheung, K.F.: Resonance in Hawaii waters from the 2006 Kuril Islands tsunami, Geophysical Research Letters, 35(7), https://doi.org/10.1029/2007GL032843, 2008.

Okada, Y.: Surface deformation due to shear and tensile faults in a half-space, Bulletin of the Seismological Society of America, 75(4), 1135-1154, 1985.

Okal, E.A.: Seismic parameters controlling far-field tsunami amplitudes: a review, Natural Hazards, 67-96, 1988.

Pallares, E., Lopez, J., Espino, M. and Sánchez-Arcilla, A.: Comparison between nested grids and unstructured grids for a high-resolution wave forecastingsystem in the western Mediterranean sea, Journal of Operational Oceanography, 10:1, 45-58, https://doi.org/10.1080/1755876X.2016.1260389, 2017.

Patriat, M., Collot, J., Danyushevsky, L., Fabre, M., Meffre, S., Falloon, T., Rouillard, P., Pelletier, B., Roach, M. and Fournier, M.: Propagation of back-arc extension into the arc lithosphere in the southern New Hebrides volcanic arc, Geochemistry Geophysics Geosystems, 16 (9), 3142-3159, 2015.

Pelletier, B., Calmant, S. and Pillet, R.: Current tectonics of the Tonga-New Hebrides region, Earth and Planetary Science Letters, 164, 263-276, 1998.

Pinto, L., Fortunato, A.B., Zhang, Y., Oliveira, A. and Sancho, F.E.P.: Development and validation of a three-dimensional morphodynamic modelling system for non-cohesive sediments, Ocean Modelling, 57-58, 1-14, http://dx.doi.org/10.1016/j.ocemod.2012.08.005, 2012.

Priest, G.R. and Allan, J.C.: Comparison of Oregon tsunami hazard scenarios to a probabilistic tsunami hazard analysis (PTHA). Oregon Department of Geology and Mineral Industries, Open-file Report 0-19-04, 94 pp., 2019.

Rabinovich, A.B.: Seiches and harbor oscillations. Handbook of Coastal and Ocean Engineering, 193-236, https://doi.org/10.1142/9789812819307_0009, 2009.

Régnier M., Deschamps A., Monfret T., Pelletier B., Pillet R., Lebellegard P., Courboulex F., Delouis B. and Gaffet S.: Stress interaction during a seismic swarm at the southern termination of the New Hebrides trench, EGU 2004 Session TS19, Nice, 29 April 2004.

Roeber, V., Yamazaki, Y. and Cheung, K.F.: Resonance and impact of the 2009 Samoa tsunami around Tutuila, American Samoa, Geophysical Research Letters 37 L21604, https://doi.org/10.1029/2010GL044419, 2010.

Roger, J., Allgeyer, S., Hébert, H., Baptista, M.A., Loevenbruck, A. and Schindelé, F.: The 1755 Lisbon tsunami in Guadeloupe Archipelago: source sensitivity and investigation of resonance effects, The Open Oceanography Journal, 4, 58-70, https://doi.org/10.2174/1874252101004010058, 2010.

Roger, J., Aucan, J., Pelletier, B., Lebellegard, P. and Lefèvre, J.: The December 5, 2018 M_w 7.5 earthquake on the south Vanuatu subduction zone: numerical modelling and development of a scenario database for New Caledonia tsunami hazard assessment, Geophysical Research Abstracts, 21, EGU2019-3210, https://meetingorganizer.copernicus.org/EGU2019/EGU2019-3210.pdf, 2019a.

https://doi.org/10.5194/nhess-2021-58
Preprint. Discussion started: 18 March 2021
© Author(s) 2021. CC BY 4.0 License.

Roger, J., Pelletier, B. and Aucan, J.: Update of the tsunami catalogue of New Caledonia using a decision table based on seismic data and marigraphic records, Natural Hazards and Earth System Sciences, 19, 1471-1483, https://doi.org/10.5194/nhess-19-1471-2019, 2019b.

Roger, J., Pelletier, B., Aucan, J. and Thomas, B.: Tsunamis in New Caledonia: from the update of the catalogue to the December 5, 2018 event. STAR 2019 Abstracts Booklet, STAR Conference, Fiji, November 19-22, 2019, http://star.gem.spc.int/docs/Abstract-booklet.pdf, 2019c.

Roland, A., Zhang, Y.L., Wang, H.V., Meng, Y., Teng, Y.-C., Maderich, V., Brovchenko, I., Dutour-Sikiric, M. and Zanke, U.: A fully coupled 3D wave-current interaction model on unstructured grids. Journal of Geophysical Research, 117, C00J33, http://doi.org/10.1029/2012JC007952, 2012.

Rouland D., Régnier M., Pillet R. and lafoy Y.: An unexpected large magnitude earthquake south of New Hebrides trench: broad band investigations and tectonic implications, AGU Fall Meeting abstract, 1995.

Sahal A., Pelletier B., Chatelier J., Lavigne F. and Schindelé F.: A catalog of tsunamis in New Caledonia from 28 March 1875 to 30 September 2009, Comptes Rendus Geoscience, 342, 437-444, 2010.

Sahal, A., Roger, J., Allgeyer, S., Lemaire, B., Hébert, H., Schindelé, F. and Lavigne, F.: The tsunami triggered by the 21 May 2003 Boumerdès-Zemmouri (Algeria) earthquake: field investigations on the French Mediterranean coast and tsunami modelling, Natural Hazards and Earth System Sciences, 9, 1823-1834, https://doi.org/10.5194/nhess-9-1823-2009, 2009.

Satake, K.: Effects of bathymetry on tsunami propagation: application of ray tracing to tsunamis, Pure and Applied Geophysics, 126(1), 27-36, https://doi.org/10.1007/BF00876912, 1988.

Shigihara, Y. and Fujima, K.: A nesting approach using unstructured grid system for numerical simulation of tsunami. Journal of Japan Society of Civil Engineers, Ser. B2, 68(2), I_186-I_190, https://doi.org/10.2208/kaigan.68.I_186, 2012.

Smith, H.F.W. and Sandwell, D.T.: Global sea floor topography from satellite altimetry and ship depth soundings, Science, 277(5334), 1956-1962, https://doi.org/10.1126/science.277.5334.1956, 1997.

Swapna, M. and Srivastava, K.: Effects of Murray ridge on the tsunami propagation from Makran subduction zone, Geophysical Journal International, 199(3), 1430-1441, https://doi.org/10.1093/gji/ggu336, 2014.

Tari, D. and Siba, G.: Brief summary of the Aneityum tsunami impact assessment report 05th December 2018, Vanuatu Meteorology and Geohazards Department report, 4 pp., 2018.

Titov, V.V.: Numerical modelling of long wave runup. Ph.D. thesis, University of Southern California, Los Angeles, California, 141 pp., 1997.

Titov, V.V., Rabinovich, A.B., Mofjeld, H.O., Thomson, R.E. and Gonzalez, F.I.: The global reach of the 26 December 2004 Sumatra tsunami. Science, 309, 2045-2048, 2005.

Titov, V.V. and Synolakis, C.E.: Modelling of breaking and nonbreaking long wave evolution and runing using VTCS-2, Journal of Waterways, Ports, Coastal and Ocean Engineering, 121(6), 308-316, 1995.

https://doi.org/10.5194/nhess-2021-58
Preprint. Discussion started: 18 March 2021
© Author(s) 2021. CC BY 4.0 License.

Titov, V.V. and Synolakis, C.E.: Numerical modelling of 3-D long wave runup using VTCS-3, in: Long Wave Runup Models, edited by Liu, P., Yeh, H. and Synolakis, C., World Scientific Publishing Co. Pte.Ltd. , Singapore, 242-248, 1996.

Titov, V.V. and Synolakis, C.E.: Extreme inundation flows during the Hokkaido-Nansei-Oki tsunami, Geophysical Research Letters, 24(11), 1315-1318, 1997.

U.S. Geological Survey: Earthquake catalog, accessed January 10, 2019 at URL https://earthquake.usgs.gov/earthquakes/search/, 2019.

Varillon, D., Fiat, S., Magron, F., Allenbach, M., Hoibian, T., De Ramon N'Yeurt, A., Ganachaud, A., Aucan, J., Pelletier, B., and Hocdé, R.: ReefTEMPS: the observation network of the coastal sea waters of the South, West and South-West Pacific, SEANOE, https://doi.org/10.17882/55128, 2018.

Vela, J., Pérez, B., Gonzalez, M., Otero, L., Olabarrieta, M., Canals, M. and Casamor, J.L.: Tsunami resonance in Palma Bay and Harbor, Majorca Island, as induced by the 2003 Western Mediterranean earthquake, The Journal of Geology, 122(2), 165-182, https://doi.org/10.1086/675256, 2014.

Vidale, J. and Kanamori, H.: The October 1980 earthquake sequence near the New Hebrides, Geoph. Res. Let., 10, 1137-1140, 1983.

Yoon, S.B., Kim, S.C., Baek, U. and Bae, J.S.: Effects of bathymetry on the propagation of tsunamis towards the east coast of Korea, Journal of Coastal Research, Special Issue 70, Proceedings of the 13th International Coastal Symposium, 332-337, https://doi.org/10.2112/SI70-056.1, 2014.

Zhang, Y.J., Ateljevich, E., Yu, H.-C., Wu, C.H. and Yu, J.C.S.: A new vertical coordinate system for a 3D unstructured-grid model, Ocean Modelling, 85, 16-31, https://doi.org/10.1016/j.ocemod.2014.10.003, 2015.

Zhang, Y.J. and Baptista, A.M.: SELFE: a semi-implicit Eulerian-Lagrangian finite-element model for cross-scale ocean circulation. Ocean modelling, 21(3–4), 71-96, http://doi.org/10.1016/j.ocemod.2007.11.005, 2008.

Zhang, Y.J., Priest, G., Allan, J. and Stimely, L.: Benchmarking an Unstructured-Grid Model for Tsunami Current Modelling. Pure and Applied Geophysics, 173, 4075-4087, https://doi.org/10.1007/978-3-319-55480-8_20, 2016b.

Zhang, Y.J., Ye, F., Stanev, E.V. and Grashorn, S.: Seamless cross-scale modelling with SCHISM. Ocean Modelling, 102, 64-81, http://doi.org/10.1016/j.ocemod.2016.05.002, 2016a.